Volume 11
Number 4
April 2026
Pages 919–1164

Nanoscale Horizons

The home for rapid reports of exceptional significance in nanoscience and nanotechnology

rsc.li/nanoscale-horizons

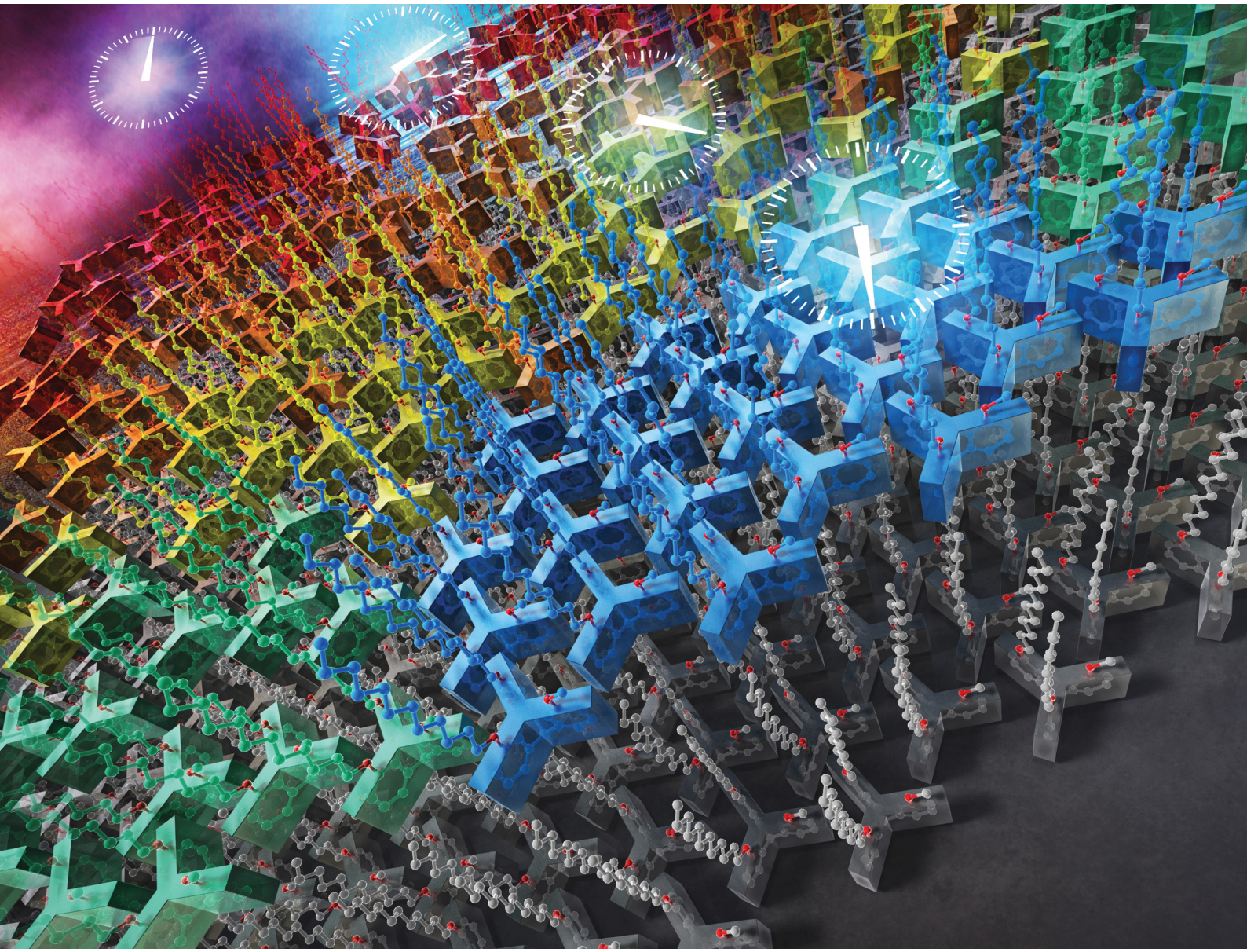

ISSN 2055-6756

ROYAL SOCIETY OF CHEMISTRY

COMMUNICATION

Go Watanabe *et al.*

Molecular dynamics insights into orientation and hexagonal ordering of tripodal triptycenes on solid surfaces

NCNST

Nanoscale Horizons

ROYAL SOCIETY OF CHEMISTRY

COMMUNICATION

View Article Online
View Journal | View Issue

Cite this: *Nanoscale Horiz.*, 2026, 11, 999

Received 22nd December 2025,
Accepted 3rd March 2026

DOI: 10.1039/d5nh00837a

rsc.li/nanoscale-horizons

Molecular dynamics insights into orientation and hexagonal ordering of tripodal triptycenes on solid surfaces

Kaito Nitta,[a] Yoshiaki Shoji,[bc] Takanori Fukushima[bc] and Go Watanabe[*ad]

Triptycene derivatives bearing long alkoxy chains at the 1,8,13- or 1,8-positions have been demonstrated to self-assemble on solid substrates into highly ordered thin films featuring a two-dimensional (2D) nested hexagonal packing of the triptycene moieties and a one-dimensional (1D) stacking layer. Although the bulk-phase structures of these derivatives have been clarified, the molecular-level mechanism governing their assembly near solid interfaces remains elusive. Here, we performed all-atom molecular dynamics (MD) simulations to investigate three triptycene derivatives (Trip1, Trip2, and Trip3) with different alkoxy-chain substitution patterns, revealing their assembly structures, thermodynamic stabilities, and interfacial ordering processes. Our simulations showed that antiparallel molecular alignment is thermodynamically stable in bulk assemblies, whereas thin films preferentially adopt a parallel alignment, indicating that solid interfaces promote this orientation. Furthermore, thermal annealing of stair-stepped trilayers drove their transformation into flat bilayers and the growth of hexagonally ordered domains, quantified by radial distribution functions and hexatic order parameters. Comparative analysis demonstrated that alkoxy substitution patterns dictate packing density, structural order, and phase stability, in excellent agreement with experimental observations. These findings provide molecular-level insights into interface-driven self-assembly and establish design principles for constructing thermodynamically stable, highly ordered organic thin films, enabling simulation-guided strategies for next-generation nanoscale materials design.

New concepts

This work introduces a new concept for controlling nanoscale ordering in organic thin films through interface-driven molecular alignment, revealed by all-atom molecular dynamics simulations. We demonstrate that solid interfaces fundamentally alter the preferred packing of triptycene derivatives, promoting parallel alignment in ultrathin films, in stark contrast to the antiparallel arrangement observed in bulk crystals. This discovery provides a mechanistic basis for designing highly ordered films at the nanoscale. Unlike previous studies that relied on empirical optimization or qualitative observations, our approach establishes quantitative and generalizable design principles linking alkoxy substitution patterns to packing density, structural order, and thermodynamic stability. By dynamically tracking the evolution of hexagonal domains during thermal annealing, we uncover how interfacial interactions and molecular architecture synergistically govern ordering processes. This concept advances nanoscience by bridging the gap between experimental thin-film fabrication and molecular-level understanding, enabling simulation-driven strategies for rational interface engineering. It offers actionable guidelines for tailoring nanoscale structures and phase stability in functional organic materials, paving the way for next-generation electronic and optoelectronic devices.

Introduction

Surface processing of the substrate is a key consideration in the fabrication of functional thin films, for both organic and inorganic materials. In the case of organic thin-film transistors (OTFTs), the interface between the dielectric layer and organic semiconductor layers plays an important role in determining the alignment of organic molecules, critically influencing the performance of OTFTs. To control this alignment, self-assembled monolayers (SAMs) are widely employed on metal and metal oxide substrates, where they realize stable and uniform surface through specific chemical interactions with the substrate. These monolayers typically consist of molecules with long alkyl chains and terminal anchoring groups that promote ordered assembly. However, direct formation of SAMs on organic substrates such as polymers remains uncommon, as these substrates often lack well-defined anchoring sites.

[a] *Department of Physics, School of Science, Kitasato University, 1-15-1 Kitazato, Minami-ku, Sagamihara, Kanagawa, 252-0373, Japan*
[b] *Laboratory for Chemistry and Life Science, Institute of Integrated Research, Institute of Science Tokyo, 4259 Nagatsuta, Midori-ku, Yokohama 226-8501, Japan*
[c] *Research Center for Autonomous Systems Materialogy (ASMat), Institute of Integrated Research, Institute of Science Tokyo, 4259 Nagatsuta, Midori-ku, Yokohama 226-8501, Japan*
[d] *Department of Data Science, School of Frontier Engineering, Kitasato University, 1-15-1 Kitazato, Minami-ku, Sagamihara, Kanagawa, 252-0373, Japan, go0325@kitasato-u.ac.jp*

A promising approach to overcome this limitation is to employ molecular systems capable of forming ordered thin films regardless of the surface composition. Fukushima and co-workers demonstrated that paraffinic triptycene derivatives with long alkoxy chains at the 1,8,13- or 1,8-positions on the rigid three-bladed propeller framework form highly ordered thin films, featuring a two-dimensional (2D) nested hexagonal packing of the triptycene cores and one-dimensional (1D) stacking layer along the molecular axis, with domain sizes reaching the order of cm^2 (Fig. 1a and b, Trip1, Trip2, and Trip3).[1–4] Importantly, the 2D triptycene arrays orient parallel to the solid surfaces on both inorganic and polymer substrates.[3] These oriented triptycene films can be fabricated *via* simple techniques such as spin-coating or thermal vacuum evaporation, making them attractive for thin-film device applications. For example, coating an approximately 5 nm-thick film of Trip2 on the surface of a parylene dielectric layer prior to organic semiconductor deposition has been shown to improve the structural order of the semiconductor layer, thereby enhancing transistor performance.[5]

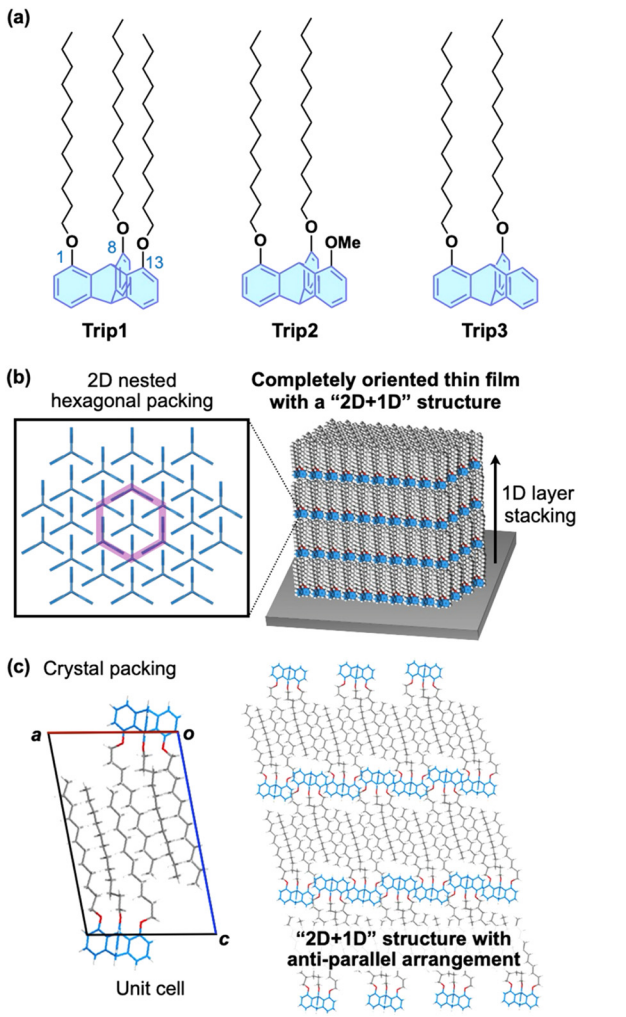

Fig. 1 (a) Molecular structures of paraffinic triptycene derivatives Trip1, Trip2, and Trip3. The blue numbers indicate the substitution positions on the triptycene moiety. (b) Schematic illustration of the assembly structure of the triptycenes in their thin films. (c) Crystal packing diagram of Trip1 with an antiparallel arrangement of neighboring molecules.

Despite these advances, elucidating the detailed molecular orientation of triptycene thin films near solid substrates has remained challenging. In the single crystal of Trip1, adjacent molecules are arranged in an alternating antiparallel fashion to form 2D layers (Fig. 1c). If this arrangement were adopted on solid surfaces, gaps at the solid–molecule interface would form. Consequently, it is more favorable for triptycene molecules within a 2D layer to adopt a parallel orientation during thin-film formation on solid substrates (Fig. 1b). This parallel orientation has been confirmed experimentally by angle-resolved time-of-flight low-energy atom scattering (TOFLAS), a surface-sensitive elemental analysis technique, for monolayer films of a triptycene derivative bearing long fluorine-terminated alkoxy side chains.[3] Nevertheless, the mechanism driving this orientation, which differs from the arrangement observed in solution-grown single crystals, remains unclear. To investigate this behavior, we employed all-atom molecular dynamics (MD) simulations, a widely used molecular simulation method.

Molecular simulations offer a powerful means to gain fundamental insights into organic thin films, revealing molecular-level details of alignment, orientation, and ordering that are often inaccessible through experimental methods alone. Such molecular simulations have been employed to investigate many aspects of organic thin films behavior, including their stability at solid or vacuum interfaces, the influence of surface morphology on molecular orientation, and the effect of anchoring on the orientational order of the molecules from the interface into the bulk.[5–14] MD simulations are also commonly used to analyze the stable structures and dynamics of molecules within thermally equilibrated molecular assemblies. They are a valuable tool for studying the thermodynamics of aggregation and assembly processes, and have been extensively applied to understand the formation of micelles, fibers, and nanotubes by amphiphilic molecules and peptides,[15–22] as well as analogous self-assembly processes of hydrophobic organic molecules.[23–27] However, relatively few MD simulation studies using all-atom models have specifically investigated the self-assembly processes of organic thin films on solid substrates.[6,28–30] Here, we report all-atom MD simulations of three paraffinic triptycenes (Trip1, Trip2, and Trip3) that form highly ordered thin films, providing insights into their molecular assembly and orientation behavior during thin-film formation.

Results and discussion

All-atom MD simulations were performed for three different triptycene derivatives, Trip1, Trip2, and Trip3, considering bulk structures with both parallel and antiparallel arrangements, as well as thin films consisting of one to four layers. The detailed procedure to construct the initial structures for these systems is explained in the SI. The snapshots of these initial structures are shown in Fig. S1 and S2, and the parameters specifying them are listed in Tables S1 and S2. The MD simulations were performed using GROMACS 2020.5. To generate the initial

structures of the monolayers on the substrate (information regarding the size of the system is listed in Table S3), monolayers of Trip1, Trip2, and Trip3 aligned in parallel and antiparallel arrangements were placed on an SiO_2 substrate.

To provide context for the following discussion, we first summarize the experimentally observed thermal stabilities of the Trip1, Trip2, and Trip3 assemblies.[3,4] Although all three derivatives form similar 2D + 1D structures (Fig. 1), their thermal stabilities differ markedly. Trip3, which bears only two dodecyloxy chains, exhibits much lower thermal stability (melting point: 134 °C)[31] than that of Trip1 (melting point: 211 °C), which bears three dodecyloxy chains.[3,4] In contrast, the 2D + 1D assembly of Trip2, in which one of the three dodecyloxy chains of Trip1 is replaced by a methoxy group, shows even higher thermal stability (melting point: 231 °C).[3] These differences in the alkoxy substitution patterns also affect the structural ordering of thin films on the macroscopic scale. Under identical vacuum deposition and thermal-annealing conditions, Trip2 forms thin films with larger terrace domains and smoother surfaces than those formed by Trip1.[3]

Beginning with analysis of the bulk assemblies, Fig. 2 illustrates MD simulation snapshots of bulk structures for Trip1 in both parallel and antiparallel configurations, with atoms colored according to their *B*-factors. In the parallel arrangement, atomic fluctuations vary significantly between layers, with some layers showing larger alkyl chain fluctuations. One layer also exhibits a detectable tilt relative to the layer normal. In contrast, the antiparallel configuration shows restricted motion, with the chains remaining uniformly oriented and only the termini of the alkyl chains fluctuating appreciably. Interdigitation of the alkyl chains suppress their rotational freedom, enhancing the thermal stability of the triptycene cores.

For both the parallel and antiparallel bulk systems of Trip2 and Trip3, the molecules were unable to form ordered, stable assemblies, and deformation of the layers was observed (Fig. S3). This is consistent with experimental results, in which no crystalline assembly structures have been observed for either Trip2 or Trip3. In the antiparallel systems, the alkyl chains exhibited much larger fluctuations than the triptycene cores. This increased mobility arises from the reduced number of long-chain alkyl substituents relative to Trip1, which creates additional free volume and prevents dense molecular packing.

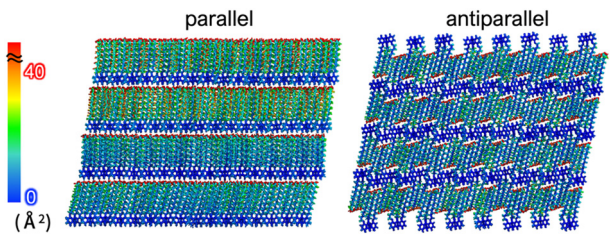

Fig. 2 MD simulation snapshots with color-coded B-factor distributions for parallel (left) and antiparallel (right) molecular alignment systems of bulk Trip1 after 100 ns equilibration runs at 300 K. Atoms are color-coded using a rainbow scale for B-factor values ranging from 0 to 40 $Å^2$, while all values exceeding 40 $Å^2$ are represented in red.

For thin films, such as monolayers and bilayers, experiments indicated that triptycene derivatives preferentially adopt a parallel configuration. Consistent with these results, Fig. 3 shows that the free-standing monolayers with parallel alignment were more stable than their antiparallel counterparts for all simulated molecules. In the parallel Trip1 systems, molecular fluctuations in the bilayer and trilayer were much lower than in the monolayer, but the four-layer film exhibited noticeable deformation. In contrast, the four-layer antiparallel film of Trip1 formed a stable structure due to the interdigitation of the flexible alkyl chains, with disorder occurring only at the interfacial triptycene groups. These findings indicate that very thin films of Trip1, such as monolayer, bilayer, or trilayer films, favor stable parallel alignment, while increasing the film thickness induces a transition toward an antiparallel arrangement. This trend was also observed for both Trip2 and Trip3, although their atomic fluctuations were larger than those of Trip1, as shown in Fig. 3.

We also performed MD simulations of the monolayers on SiO_2 substrates for direct comparison with experimental studies conducted on solid substrates. As shown in Fig. 4, monolayers with parallel molecular alignment remained flat and uniform for all the simulated triptycene derivatives, without collapsing, condensing, or exhibiting large fluctuations. In the parallel Trip1 monolayer, large fluctuations were only observed at the termini of the alkyl chains, while Trip2 and Trip3 exhibited more significant fluctuations and greater orientational disorder. In the antiparallel Trip1 monolayer, the molecular orientation remains ordered, but the thermal fluctuations of individual molecules were large. Order was not maintained in the antiparallel Trip2 and Trip3 monolayers. There are no significant differences in the packings of the triptycene cores among Trip1, Trip2, and Trip3. Overall, these results indicate that parallel alignment is more favorable than antiparallel alignment for triptycene monolayers on solid substrates, consistent with the available experimental observations.

The interactions between the tripodal triptycenes and the hydrogen-terminated SiO_2 surface are dominated by van der Waals interactions. Our results indicate that the parallel orientation is energetically favorable on the substrate because it maximizes the contact area of the triptycene moieties with the surface, thereby increasing the van der Waals stabilization. This is also supported by the fact that the antiparallel arrangement would form gaps at the solid–molecule interface, reducing the effective interaction area.

Previous atomic force microscopy (AFM) measurements of spin-coated Trip1 films showed that the molecules aligned perpendicular to the substrate in parallel and formed multilayered pyramidal hexagons.[3] AFM analyses of evaporated Trip1 films further revealed that films with initial thicknesses of tens of nanometers became flat after thermal annealing, with the observed height difference falling within the thickness of two molecular layers. These observations suggest that the initial stair-stepping multilayers condense into flatter structures upon annealing. Trip2 has also been reported to form thin, flat films with higher phase stability than that of Trip1, maintaining its structure from room temperature up to 504 K.[3] To investigate

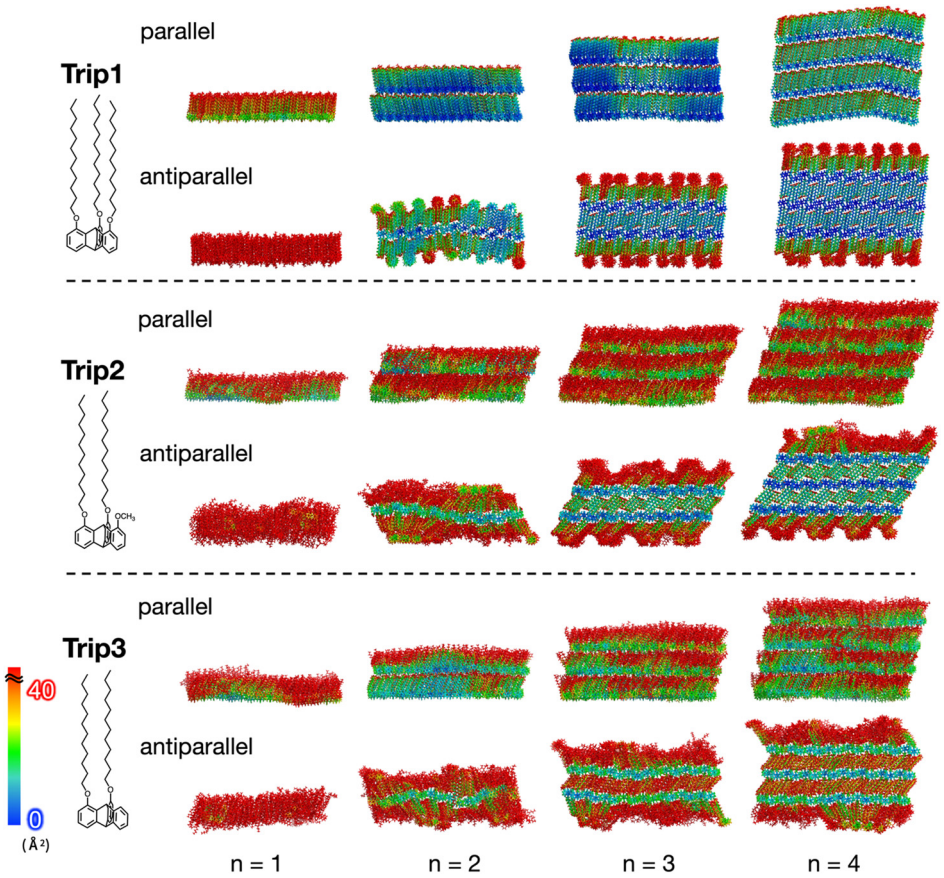

Fig. 3 Color-coded *B*-factor distributions mapped onto MD simulation snapshots of Trip1, Trip 2, and Trip3, after the 100 ns equilibration runs. For each molecule, the snapshots show thin films composed of 1, 2, 3, and 4 layers in both parallel and antiparallel alignments. Atoms are color-coded using a rainbow scale for *B*-factor values ranging from 0 to 40 Å^2, while all values exceeding 40 Å^2 are represented in red.

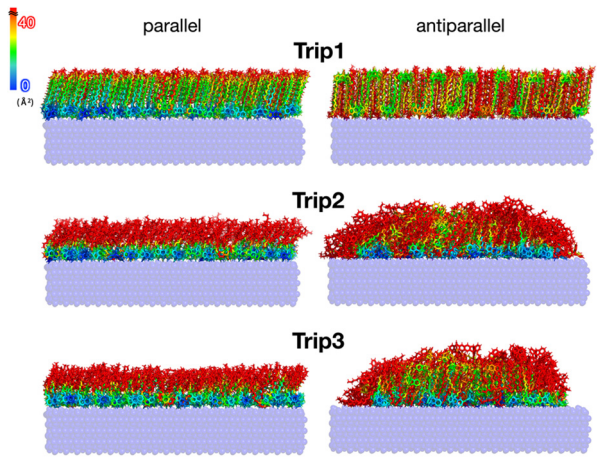

Fig. 4 MD simulation snapshots of Trip1, Trip2, and Trip3 monolayers on the SiO_2 substrates after 100 ns equilibration runs, with *B*-factor distributions color-coded. Initial molecular orientations within the monolayers were parallel and antiparallel for the left and right snapshots, respectively.

the thermal stability of the parallel molecular alignment in triptycene thin films, we performed MD simulations of the annealing process. First, the pre-equilibration run was done for 5 ns at 300 K and 400 K. Then, we conduct the equilibration run for 1000 ns at 400 K for a stair-stepping trilayer of Trip2, as shown in Fig. 5 and Movie S1. The details are available in the SI. After 10 ns of the equilibration, the triptycene groups in the top layer partially mixed with those in the middle layer, producing coexisting domains of densely and sparsely packed molecules. The initial hexagonal packing of the middle layer was lost, and the alkyl chains adopted random orientations. The radial distribution function (RDF) for the upper layer at this stage showed no positional order, as shown in Fig. 6(a). By 100 ns, the ordering of the triptycene groups was partially reconstructed, with small domains exhibiting hexagonal packing of the triptycene groups. The RDF for the upper layer at 100 ns, as shown in Fig. 6(b), differed significantly from that at 10 ns, displaying a sharp first peak and a few periodic peaks. After 1000 ns of the thermal annealing, the hexagonally ordered domain in the upper layer had grown substantially, and the molecules became more uniformly distributed. This improved positional order is reflected in the RDF, showing a sharp peak and clear periodicity of each subsequent peak (Fig. 6(c)). Notably, the first RDF peak at approximately 0.8 nm corresponds with the hexagonal lattice parameter obtained from previous X-ray diffraction studies. This in-plane positionally ordered domain is therefore a result of annealing and not due to the arbitrariness of the initial structure.

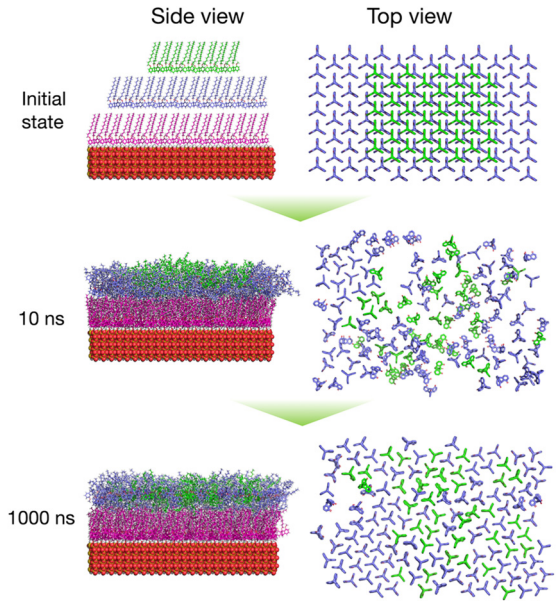

Fig. 5 MD simulation snapshots of the stair-stepping trilayer of Trip2 on the SiO_2 substrate during the annealing process. The snapshots show side views of the entire trilayer and substrate (left), and top views focusing on the triptycene moieties within the upper two layers (right).

The growth of the hexagonally ordered domain in the upper layer was also quantified by analyzing the hexatic order parameter $\psi = \psi_6(\mathbf{r}_k)$, for each triptycene molecule k and its neighboring molecules within 0.9 nm (see the SI for details). As shown in Fig. 6(d) and (e), at 100 ns, there were 40 molecules out of the total 138 molecules in the upper layer with a high degree of local six-fold symmetry (ψ = 0.8–1.0), and 20 molecules with high disorder (ψ = 0.0–0.2). By contrast, at 1000 ns, these numbers were 60 and 10, respectively. About 100 molecules exhibited ψ greater than 0.6 after 1000 ns, indicating that a substantial fraction of the upper layer became highly hexatically ordered during the annealing process.

For Trip1, the annealing simulation produced a different outcome. While the molecules in the top and middle layers merged into a single layer, the assembly of the original middle layer remained largely intact, with the molecules from the top layer occupying the surrounding free volume as shown in Fig. S4. The reformed layer adopted a parallel molecular alignment, but contained disordered regions primarily composed of molecules originating from the top layer. This behavior reflects the dense alkyl chain packing in Trip1, which prevents the ordered domain of the middle layer from reconstructing through mixing with the top layer molecules. Both the molecular ordering and uniformity of the top layer obtained after annealing were much lower for Trip1 than for Trip2. These findings align with the previous experimental results suggesting that Trip2 forms highly oriented and uniformly flat thin films with superior phase stability.

While the annealing simulation was also performed for Trip3, its stepped trilayer did not reach equilibrium within the accessible timescale of the all-atom MD simulations. Therefore, it could not be analyzed in the same manner as Trip1 and Trip2. Since the parallel monolayer of Trip3 on SiO_2 was found to be stable, a possible alternative equilibration strategy would

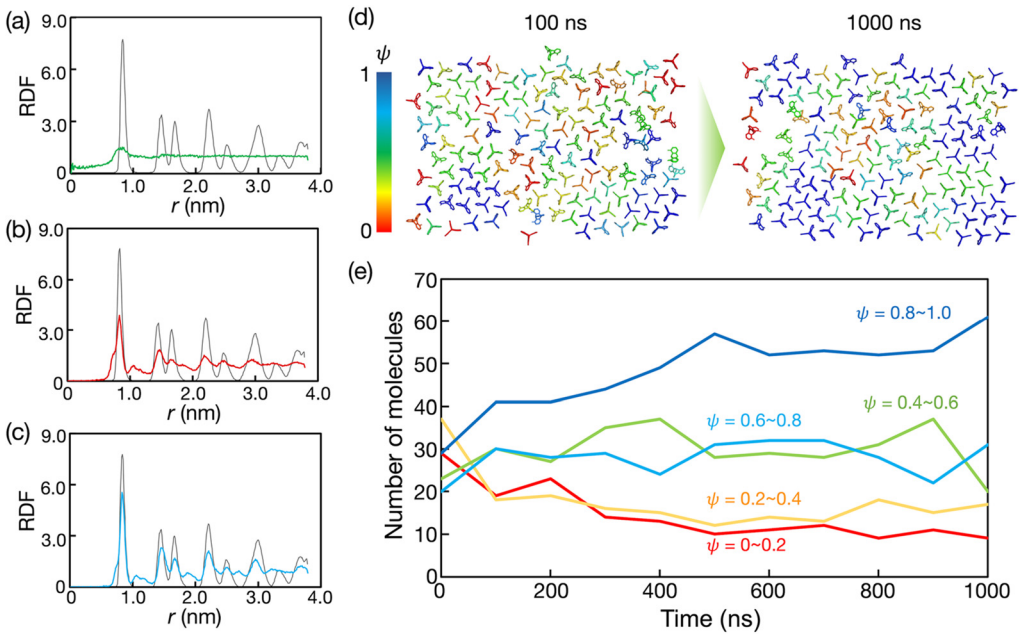

Fig. 6 Radial distribution functions (RDFs) for triptycene moieties in Trip2 during the annealing process of MD simulation: (a) green, (b) red, and (c) blue curves represent RDFs at 10 ns, 100 ns, and 1000 ns, respectively and black lines show those derived from the ideal hexagonally ordered structure constructed based on the crystal structure. (d) Color-coded distributions of the hexatic order parameter (ψ) mapped onto MD simulation snapshots of triptycene moieties at 100 ns and 1000 ns during the annealing simulation equilibration run. (e) Time evolution of the number of molecules categorized by their ψ values. The number of molecules with ψ values in the ranges of 0–0.2, 0.2–0.4, 0.4–0.6, 0.6–0.8, and 0.8–1.0 are represented by red, yellow, green, sky-blue, and blue curves, respectively.

be to perform annealing simulations in a stepwise, layer-by-layer manner, sequentially equilibrating the monolayer, bilayer, and trilayer structures to facilitate relaxation toward an equilibrated multilayer state.

Conclusion

In this study, we performed all-atom MD simulations to investigate the thermodynamically preferred assembly structures of three triptycene derivatives bearing different numbers of dodecyloxy and methoxy chains. The simulations were conducted under several conditions, including bulk crystals, thin films in a vacuum ranging from monolayers to four-layer films, and monolayers on an SiO_2 substrate. In the bulk crystal structure, an antiparallel arrangement, where adjacent molecules adopt opposite alignment, was confirmed to be the most thermodynamically stable for all three derivatives. In contrast, ultrathin films such as monolayers and bilayers favor a parallel alignment, consistent with the experimentally observed differences between bulk and thin film structures. Monolayers on SiO_2 also maintained a stable parallel orientation for all three derivatives, providing insight into molecular orientation at solid-organic interfaces. Simulation of the annealing process further revealed distinct molecular-level rearrangement processes among the derivatives. For Trip2, annealing a stair-stepping trilayer produced a flat bilayer, in which hexagonally ordered domains of triptycene moieties developed and expanded over time. After a 1000 ns simulation, the annealed Trip2 film exhibited high hexatic order and uniform molecular distribution. In contrast, Trip1 retained disordered regions associated with incomplete reorganization, in agreement with experimental reports that Trip2 forms more uniformly ordered and phase-stable thin films.

Overall, our MD simulations demonstrate that dense packing of triptycene moieties in combination with the parallel alignment of long alkyl chains are dominant structural features governing the stability and order of triptycene-based thin films. These molecular-level pictures provide access to static properties such as molecular alignment and dynamic processes such as film formation that are difficult to observe directly even with state-of-the-art experimental techniques, including advanced scanning probe microscopies. Therefore, the present work offers guidelines for the rational design of structurally elaborated molecular thin films, which in turn facilitate the development of high-performance functional organic thin films and devices.

Author contributions

G. W. and T. F. conceived the project. K. N. performed molecular dynamics simulations and analyzed the data. Y. S. and T. F. helped to analyze and discuss the simulation data. Y. S., T. F., and G. W. cowrote the manuscript. All authors have given approval to the final version of the manuscript.

Conflicts of interest

There are no conflicts to declare.

Data availability

Data are available from the authors upon request.

The data supporting this article have been included as part of the supplementary information (SI). Supplementary information is available. See DOI: https://doi.org/10.1039/d5nh00837a.

Acknowledgements

This work was supported by JSPS KAKENHI (JP22K18953 to G. W. and JP21H05024, JP21H04690, and JP20H05868 to T. F.) and JST CREST (JPMJCR24S1 and JPMJCR23O1 to G. W.). This work was also supported in part by the Research Program of ''Five-Star Alliance'' in ''NJRC Mater. & Dev.''. The computations were partially performed at the Research Center for Computational Science, Okazaki, Japan (Project: 22-IMS-C043, 23-IMS-C038, 24-IMS-C038, and 25-IMS-C039).

References

1 M. Zharnikov, Y. Shoji and T. Fukushima, *Acc. Chem. Res.*, 2025, **58**, 312–324.
2 F. Ishiwari, Y. Shoji, C. J. Martin and T. Fukushima, *Polym. J.*, 2024, **56**, 791–818.
3 N. Seiki, Y. Shoji, T. Kajitani, F. Ishiwari, A. Kosaka, T. Hikima, M. Takata, T. Someya and T. Fukushima, *Science*, 2015, **348**, 1122–1126.
4 M. Kumano, M. Ide, N. Seiki, Y. Shoji, T. Fukushima and A. Saeki, *J. Mater. Chem. A*, 2016, **4**, 18490–18498.
5 T. Yokota, T. Kajitani, R. Shidachi, T. Tokuhara, M. Kaltenbrunner, Y. Shoji, F. Ishiwari, T. Sekitani, T. Fukushima and T. Someya, *Nat. Nanotechnol.*, 2018, **13**, 139–144.
6 R. G. D. Valle, E. Venuti, A. Brillante and A. Girlando, *Chem. Phys. Chem.*, 2009, **10**, 1783–1788.
7 M. Ando, T. B. Kehoe, M. Yoneya, H. Ishii, M. Kawasaki, C. M. Duffy, T. Minakata, R. T. Phillips and H. Sirringhaus, *Adv. Mater.*, 2015, **27**, 122–129.
8 M. Sadati, H. Ramezani-Dakhel, W. Bu, E. Sevgen, Z. Liang, C. Erol, M. Rahimi, N. Taheri Qazvini, B. Lin, N. L. Abbott, B. Roux, M. L. Schlossman and J. J. De Pablo, *J. Am. Chem. Soc.*, 2017, **139**, 3841–3850.
9 O. M. Roscioni, L. Muccioli and C. Zannoni, *ACS Appl. Mater. Interfaces*, 2017, **9**, 11993–12002.
10 H. Ramezani-Dakhel, M. Rahimi, J. Pendery, Y. K. Kim, S. Thayumanavan, B. Roux, N. L. Abbott and J. J. De Pablo, *ACS Appl. Mater. Interfaces*, 2018, **10**, 37618–37624.
11 T. Okamoto, M. Mitani, C. P. Yu, C. Mitsui, M. Yamagishi, H. Ishii, G. Watanabe, S. Kumagai, D. Hashizume, S. Tanaka, M. Yano, T. Kushida, H. Sato, K. Sugimoto, T. Kato and J. Takeya, *J. Am. Chem. Soc.*, 2020, **142**, 14974–14984.

12 S. Kumagai, H. Ishii, G. Watanabe, T. Annaka, E. Fukuzaki, Y. Tani, H. Sugiura, T. Watanabe, T. Kurosawa, J. Takeya, T. Okamoto and S. Kumagai, *Chem. Mater.*, 2020, **32**, 9115–9125.
13 O. M. Roscioni, L. Muccioli, A. Mityashin, J. Cornil and C. Zannoni, *J. Phys. Chem. C*, 2016, **120**, 14652–14662.
14 Z. Tian, J. Wen and J. Ma, *J. Chem. Phys.*, 2013, **139**, 014706.
15 C. Guo, Y. Luo, R. Zhou and G. Wei, *Nanoscale*, 2014, **6**, 2800–2811.
16 P. W. J. M. Frederix, G. G. Scott, Y. M. Abul-Haija, D. Kalafatovic, C. G. Pappas, N. Javid, N. T. Hunt, R. V. Ulijn and T. Tuttle, *Nat. Chem.*, 2015, **7**, 30–37.
17 N. Brown, J. Lei, C. Zhan, L. J. W. Shimon, L. Adler-Abramovich, G. Wei and E. Gazit, *ACS Nano*, 2018, **12**, 3253–3262.
18 I. W. Fu, C. B. Markegard and H. D. Nguyen, *Langmuir*, 2015, **31**, 315–324.
19 O. S. Lee, V. Cho and G. C. Schatz, *Nano Lett.*, 2012, **12**, 4907–4913.
20 H. Kuramochi, Y. Andoh, N. Yoshii and S. Okazaki, *J. Phys. Chem. B*, 2009, **113**, 15181–15188.
21 A. Ishida, G. Watanabe, M. Oshikawa, I. Ajioka and T. Muraoka, *Chem. – Eur. J.*, 2019, **25**, 13523–13530.
22 A. Yaguchi, M. Oshikawa, G. Watanabe, H. Hiramatsu, N. Uchida, C. Hara, N. Kaneko, K. Sawamoto, T. Muraoka and I. Ajioka, *Nat. Commun.*, 2021, **12**, 6623.
23 F. Chami and M. R. Wilson, *J. Am. Chem. Soc.*, 2010, **132**, 7794–7802.
24 M. Yoneya, T. Yamaguchi, S. Sato and M. Fujita, *J. Am. Chem. Soc.*, 2012, **134**, 14401–14407.
25 E. Beltrán, M. Garzoni, B. Feringán, A. Vancheri, J. Barberá, J. L. Serrano, G. M. Pavan, R. Giménez and T. Sierra, *Chem. Commun.*, 2015, **51**, 1811–1814.
26 Y. Ishii, N. Matubayasi, G. Watanabe, T. Kato and H. Washizu, *Sci. Adv.*, 2021, **7**, 1–15.
27 S. Sato, B. Dhara, D. He, D. Miyajima and G. Watanabe, *Chem. Commun.*, 2025, **61**, 4951–4954.
28 A. J. Bourque, C. R. Locker and G. C. Rutledge, *J. Phys. Chem. B*, 2017, **121**, 904–911.
29 M. Yoneya, M. Kawasaki and M. Ando, *J. Phys. Chem. C*, 2012, **116**, 791–795.
30 L. Muccioli, G. D'Avino and C. Zannoni, *Adv. Mater.*, 2011, **23**, 4532–4536.
31 M. Kondo, T. Kajitani, T. Uemura, Y. Noda, F. Ishiwari, Y. Shoji, T. Araki, S. Yoshimoto, T. Fukushima and T. Sekitani, *Sci. Rep.*, 2019, **9**, 9200.